1   Particle number size distribution and new particle formation under influence of

2   biomass burning at a high altitude background site of Mt. Yulong (3410m) in China

4 Dongjie Shang[1], Min Hu[1, 2]*, Jing Zheng[1], Yanhong Qin[1], Zhuofei Du[1], Mengren Li[1],

5 Jingyao Fang[1], Jianfei Peng[1], Yusheng Wu[1], Sihua Lu[1], Song Guo[1]*

6 [1]State Key Joint Laboratory of Environmental Simulation and Pollution Control,

7 College of Environmental Sciences and Engineering, Peking University, Beijing,

8 100871, China

9 [2]Beijing Innovation Center for Engineering Sciences and Advanced Technology,

10 Peking University, 100871, Beijing, China

12 * Corresponding author: E-mail address: minhu@pku.edu.cn, guosong@pku.edu.cn

13 **Abstract**

14   Biomass burning (BB) activities have a great impact on particle number size

15 distribution (PNSD) in upper troposphere of Tibet-Plateau, which could affect regional

16 and global climate. The intensive campaign for the measurement of PNSD, gaseous

17 pollutants and meteorological parameters was conducted at Mt. Yulong, a high-altitude

18 site (3410 m a. s. l.) in the southeast of Tibet Plateau during the pre-monsoon season

19 (22 March to 15 April), when the intensive BB activities in South Asia were observed

20 by fire maps. Long-range transport of BB pollutants could increase the accumulation

21 mode particles in background atmosphere of Mt. Yulong. As a consequence, cloud

22 condensation nuclei (CCN) concentration was found to be 2-8 times higher during BB

23 periods than that during clean period. Apart from BB, variation of planet boundary layer

24 (PBL) and new particle formation were other factors that influenced PNSD. However,

25 only 3 NPF events (with a frequency of 14 %) were observed at Mt. Yulong. Occurrence

26 of NPF events during clean episode corresponded with elevated PBL or transported BB

27 pollutants. Due to lack of condensable vapors including sulfuric acid and organic

28 compounds, the newly formed particles were not able to grow to CCN size. Our study

29 emphasized the influences of BB on aerosol and CCN concentration in atmosphere of

30 Tibet Plateau. These results can improve our understanding of the variation of particle

31 concentration in upper troposphere, and provide information for regional and global

32 climate models.

33 Key words: Tibet-Plateau, particle number size distribution, biomass burning,

34 CCN, new particle formation

35 **1.** Introduction

36 The aerosol particles can influence the radiation of the planet surface through

37 scattering the sunlight, and cloud albedo by serving as cloud condensation nuclei (CCN)

38 (IPCC, 2013). The cloud albedo effect of aerosols provides the biggest uncertainties in

39 global climate models (IPCC, 2013), and depends strongly on number concentration

40 and size of particles. Numerous studies concentrated on monitoring particle number

41 size distribution (PNSD) within the planet boundary layer (PBL), where anthropogenic

42 sources have strong impacts (Peng et al., 2014). While the particles in pristine free

43 troposphere (FT) were rarely studied. Particles in FT mainly originated from lifting of

44 emission within PBL by convective, frontal, and orographic lifting (Okamoto and

45 Tanimoto, 2016), or atmospheric nucleation. Those particles have longer lifetime and

46 could be transported in a longer distance, during which they could exchange with PBL

47 (Shen et al., 2016;D'Andrea et al., 2016). Hence, studies on FT are important because :

48 1) CCN in FT could influence cloud albedo more directly compared to surface CCN; 2)

49 FT served as a route of long-range transport of pollutants. Aircraft study is a direct way

50 to measure the FT particles, but it is costly and can only provide data within short

51 periods. Therefore, measurement at high mountain sites is one common method to study

52 the FT particles and analyze the influences of pollution transport on FT (Shen et al.,

53 2016).

54 Particles originated from BB in South Asia could have impacts on vast

55 atmosphere of Tibet Plateau by transport in FT. As the highest plateau in the world,

56 Tibet Plateau has very few anthropogenic sources, and could be taken as the continent

57 background. However, recent studies revealed that the smoke plume in South Asia

58 could ascend to FT, and transport to Himalayas and the mountain valley of Tibet Plateau

59 during pre-monsoon season (Cong et al., 2015;Lüthi et al., 2015;Bukowiecki et al.,

60 2016). During pre-monsoon season, the enhanced convection and steep pressure

gradient across the Himalaya-Gangetic region could rise the BB particles to higher altitude (Gautam et al., 2009;Adak, 2014). The particles could be transported by dry westerly, and have impacts on aerosols in Tibet Plateau region (Bonasoni et al., 2010;Chen et al., 2014). Former studies verify South Asian BB's influence in Tibet Plateau by chemical analysis of K^+, levoglucosan, etc. However, there was limited information of variation of PNSD under influence of BB. Also, there were limited studies concerning the contribution of BB to CCN in Tibet Plateau.

Except primary emissions, new particle formation (NPF) is another important source of particles in FT, but with limited measurement. According to model results, nucleation in FT contribute to 35 % of the CCN globally (Merikanto et al., 2009). Considering the level of pre-existing particles in FT is relatively low, it should provide a good condition for nucleation of the nanoparticles. As a result, NPF has been observed to happen frequently in FT, including Mt. Tai (1500m a.s.l.) (Shen et al., 2016), Mediterranean Sea (1000m-300m a.s.l.) (Rose et al., 2015), Mt. Puy de Dôme (1465 m a.s.l), Mt. Izana (2367m a.s.l.) (Rodríguez et al., 2009;García et al., 2014), Colorado Rocky Mountains (2900m a.s.l.) (Boy et al., 2008), etc. While NPF events happened less frequently at Indian foothill Himalayas (2080m) (Neitola et al., 2011). Studies at mountain sites considered that the frequency of NPF corresponded to the rise of PBL height, which could raise the concentration of anthropogenic SO_2, NH_3 and other nucleation precursors. Mechanisms of formation and the growth of nanoparticles in FT remain ambiguous (Bianchi et al., 2016), thus comprehensive measurements of PNSD as well as trace gases at high-mountain sites are necessary to provide information around this topic.

This study aimed to: 1) investigate the influence of BB from South Asia on PNSD and CCN concentration at South east of Tibet Plateau; 2) characterize the NPF at high-mountain sites. For purposes of these, a comprehensive measurement was conducted at a background site in Mt. Yulong (3410 m a.s.l.), during the pre-monsoon season.

2. Experiments and data analysis

89   2.1 Monitoring site

90   An intensive field campaign was conducted during 22 March to 15 April, at a high

91   mountains site of Mt. Yulong (27.2N, 100.2E) in Southwest China and Southeast corner

92   of Tibet Plateau, with an altitude of 3410 m a. s. l. This site is one of national regional

93   background sites coordinated by the Chinese Environmental Monitoring Center

94   (CEMC), which is a remote site on the transport route of South Asian pollutants during

95   pre-monsoon season. At the foot of the Mt. Yulong, 36 km to the south of the site is the

96   famous Lijiang Old Town, a populated tourist place. More details of the monitoring site

97   can be found in another paper (Zheng et al., 2017).

98   2.2 Instrumentation

99   PNSD was measured with a time resolution of 5 min, by two set of scanning

100   mobility particle sizer (SMPS, TSI Inc., St. Paul, MN, USA) and an aerodynamic

101   particle sizer (APS, TSI model 3321, TSI Inc., St. Paul, MN, USA). The first set of

102   SMPS consisted of a short differential mobility analyzer (DMA, Model 3085) and an

103   ultra-condensing particle counter (UCPC, Model 3776, flowrate 1.5 L/min) was used

104   to measure the 3-60 nm particles. Another SMPS with long DMA (Model 3081) and

105   normal CPC (Model 3022, flow rate 0.3 L/min) was used for measuring 60-700 nm

106   particles. A silicon diffusion tube was placed before the SMPS, controlling the relative

107   humidity of sampling air under 35 %. Diffusion loss and multiple charging calibration

108   of the particles was done for SMPS data. APS with flow rate of 1 L/min was used for

109   measuring 0.5-10 μm particles. The result of APS was modified to stokes diameter

110   assuming the particle density to be 1.7 $μg/m^3$ before combining with SMPS data. A

111   bypass flow was added before the inlet cutoff, to meet the working flow rate of the

112   PM_{10} cyclone (16.7 L/min).

113   To investigate the BB influences in aerosols, a high-resolution time-of-flight aerosol

114   mass spectrometer (HR-TOF-AMS) was deployed to measure the chemical

115   composition of aerosols. Through this instrument, we can obtain the concentration of

116   nitrate, sulfate, ammonium, chloride and high-resolution mass spectrum of organics,

especially the fragments of BB organic markers. Black carbon (BC) is another important marker for combustion sources. In this study, BC was measured with an aethalometer (Magee Scientific, USA, type AE31), by collecting aerosol particles on a filter stripe, and analyzing the transmission of the lights with seven wave length, from 370 to 950 nm. BC concentration was calculated as a multiple of the light absorption coefficient at 880nm, with the default mass attenuation cross sections of 16.6 m^2 g^{-1} (Fröhlich et al., 2015). To get the concentration of organic tracers of the new particle formation, an online-gas chromatography coupled with mass spectrometer and flame ionization detectors (GC-MS/FID) was used to measure the non-methane hydrocarbons (NMHCs), including benzene, toluene, monoterpene, etc.

Meteorological parameters, $PM_{2.5}$ and trace gases were also measured by online instruments during the campaign (Table S1). NO and NO_2 measurement was conducted by a commercial instrument (Thermo Electron model 42i NO-NO_2-NO_x analyzer) with Chemiluminescence technique. NO_2 was deoxidized to NO by a molybdenum catalyzer before detection. O_3 measurement was performed by ultraviolet (UV) absorption with Thermo Electron model 49i. CO was detected by an infrared spectrophotometry (Thermo Electron models 48i-TLE). SO_2 was measured by a commercial instrument (Thermo Electron models 43i-TLE) with ultraviolet fluorescence method. Due to the noise of the instrument and the quite low concentration of SO_2, the relative uncertainties of SO_2 measurement was high for data under 0.05 ppb.

2.3 Data processing

2.3.1 Backward trajectory analysis

The 48h backward trajectories of the air mass were computed at 4000 m a.s.l. (600 m above the ground of the Mt. Yulong site) by the Weather Research and Forecasting (WRF) model (version 3.61) to identify the impacts from South Asia. The fire spots were obtained from the satellite map from Moderate Resolution Imaging Spectroradiometer (MODIS) (https://firms.modaps.eosdis.nasa.gov/firemap/). In order

145   to characterize the air mass origin during the NPF events, the 48h backward trajectories

146   at 600 m above the ground were calculated by NOAA HYSPLIT 4 (Hybrid Single-

147   Particle Lagrangian Integrated Trajectory) model (Draxier and Hess, 1998).

148

149   2.3.2 Parameterization of NPF

150   The data of each PNSD during NPF was fitted as the sum of three or two mode

151   lognormal distribution (Hussein et al., 2005), including the geometric mean diameter

152   D_m, geometric standard deviation σ_m and total number concentration of each mode.

153   During the NPF events, the growth rate (GR) was calculated as the variation of the

154   mean diameter D_m of newly formed mode in unit internal:

155
$$GR = \frac{\Delta D_m}{\Delta t} \tag{1}$$

156   Formation rate was calculated for nucleation fraction of the particles (3-25 nm), with

157   the formula:

158
$$J_{3-25} = \frac{dN_{3-25}}{dt} + N_{3-25} \cdot CoagS_8 + F_{growth} \tag{2}$$

159   in this formula, $N_{3\text{-}25}$ is number concentration of particles within size range of 3-25 nm,

160    $CoagS_8$ is the coagulation rate of particles with diameter of 8 nm, which is the geometric

161   mean of 3-25 nm. The coagulation rate was calculated as:

162
$$CoagS(D_p) = \int K(D_p, D_p')n(D_p')dD_p' \tag{3}$$

163   in which $n(D_p')$ is number concentration of particles with size of D_p', $K(D_p, D_p')$

164   is the coagulation coefficient between D_p and D_p' particles. During nucleation events,

165   there were negligible particles that grew beyond 25 nm, so the last term in formula of

166   was not included (Dal Maso et al., 2005). To quantify the limitation of NPF from pre-

167   existing particles, the condensation sink was calculated as:

168
$$CS = 2\pi D \sum_i \beta \cdot D_i \cdot N_i \tag{4}$$

169   where D is the diffusion coefficient of the condensational vapor, e.g. sulfuric acid, β the

170   transitional regime correction factor, D_i and N_i are the diameter and number

171   concentration of particles in class i. In calculation described above, all diameters were

172 dry diameter directly measured from SMPS, so the coagulation and condensation sink

173 could be underestimated.

174   Sulfuric acid was thought to be the most important precursor of NPF events (Sipilä

175 et al., 2010), and could contribute to particle growth by condensation (Yue et al.,

176 2010;Zhang et al., 2012). In this study, the content of H_2SO_4 was calculated by a

177 pseudo-steady state method (Kulmala et al., 2001):

178 $$[H_2SO_4]=k \cdot [OH][SO_2]/CS \tag{5}$$

179 in which [OH] and $[SO_2]$ are number concentration of OH radicals and SO_2, value of k

180 is 10^{-12} cm^3s^{-1}. [OH] was estimated by:

181 $$[OH] = a(JO^1D)^{\alpha}(J_{NO2})^{\beta} \frac{b[NO_2]+1}{c[NO_2]^2+d[NO_2]+1} \tag{6}$$

182 in which $\alpha=0.83$, $\beta=0.19$, $a=4.1\times10^9$, $b=140$, $c=0.41$, $d=1.7$ (Ehhalt and Rohrer, 2000).

183 Contribution of sulfuric acid condensation to particle growth was calculated by Yue et

184 al's (2010) method.

185 2.3.3 Calculation of CCN concentration

186   In order to evaluate the variation of indirect climate effects of the particles at Mt.

187 Yulong, CCN number concentration was estimated from data of PNSD and particle

188 chemical composition. Firstly, the SNA (sulfate, nitrate, ammonium) was ion-coupled

189 to get exact chemical compounds of the inorganic salts in particles. NH_4NO_3, H_2SO_4,

190 NH_4HSO_4 and $(NH_4)_2SO_4$ were calculated following the formula:

191 $$n_{NH_4NO_3}=n_{NO_3^-},$$

192 $$n_{H_2SO_4}=\max(0, n_{SO_4^{2-}}-n_{NH_4^+}+n_{NO_3^-}),$$

193 $$n_{NH_4HSO_4}=\min(2n_{SO_4^{2-}}-n_{NH_4^+}+n_{NO_3^-}, n_{NH_4^+}-n_{NO_3^-}),$$

194 $$n_{(NH_4)_2HSO_4}=\max(n_{NH_4^+}-n_{NO_3^-}-n_{SO_4^{2-}}, 0),$$

195 where n is the mole number of the specific compounds (Gysel et al., 2007). Based on

196 κ-Köhler theory and Zdanovskii–Stokes–Robinson (ZSR) mixing rule, the hygroscopic

197 parameter of mixed particles can be calculated as (Petters and Kreidenweis, 2007):

198 $$\kappa=\sum_1^n \varepsilon_m \kappa_m$$

where ε_m is the volume fraction of the composition m in particles, and κ_m is the hygroscopic parameter of pure composition m. In this research, we consider secondary inorganic ions, organics and BC as majority composition of particles, and put them into the ZSR mixing formula. The correlated parameters of the compounds we used are in table 1.

Based on κ-Köhler theory, the relationship between κ and D_c under certain supersaturation (S_c) is:

$$\kappa = \frac{4A^3}{27D_c^3 \ln^2 S_c}, \quad A = \frac{4\sigma_{s/a}M_w}{RT\rho_W}$$

in which $\sigma_{s/a}$ is the surface tension of water, M_w and ρ_W is the molecular weight and density of water respectively, R is 8.317 J mol^{-1} K^{-1}, T is the ambient temperature. With the κ of the particles, the critical diameter D_c of the CCN activation can be achieved with this formula. Then the number concentration of CCN can be calculated as number concentration of particles larger than D_c.

3. Results and discussion

3.1 Particle number size distribution

3.1.1 Particle and meteorology parameters

Fig.1 shows the time series of PNSD and correlating meteorological parameters. Temperature and relative humidity was 6.1±3.5 °C and 54.9±19.7 %, respectively (Fig.1b). Southeast wind was dominant during the campaign, followed by South wind and Southwest wind. Average wind speed was 2.9±1.8 m/s (Fig S1). Most of the monitoring days were sunny, in favor of nucleation process, while short time rainfall occurred on 24, 26 March and 4, 6, 7, 8, 10, 11 April. During April 12, there was a heavy snow with the RH more than 90 %.

As a background high altitude site in TP, Mt. Yulong site revealed the feature of low particle concentration and strong oxidation capacity. On average $PM_{2.5}$ was 10.51±9.16 μg/m^3, similar with the results on Northeast slope of Tibet Plateau (Xu et

al., 2014;Du et al., 2015). This result was only 1/10-1/3 of that in the atmosphere of urban and rural regions in China, indicating a background situation in Southwest China (Zheng et al., 2016). However, the $PM_{2.5}$ at Yulong background site during the monsoon season was around 3 times as that at Qilian Shan Station (4180 m a.s.l.) in Northeast of Tibet Plateau (Xu et al., 2015) and at Jungfraujoch (3580 m a.s.l.), Switzerland (Bukowiecki et al., 2016), with similar altitude, indicating relatively stronger anthropogenic influence in in this area. During 22 to 30 March, 4 to 5 April and 11 to 12 April, particle mass concentration exceeded 10 μg/m^3, building up a pollution episode.

During the measurement, ozone level was 50.1±7.0 ppbv, similar with the results at high mountain sites in Europe (Cristofanelli et al., 2016;Okamoto and Tanimoto, 2016), higher than the results in Beijing during spring. This indicate that atmosphere at Mt. Yulong site had higher oxidation capacity for secondary transformation of pollutants. The concentration of NO_x and NO was 0.94±0.62 ppbv and 0.07±0.05 ppbv, respectively. SO_2 concentration was 0.06±0.05 ppbv, around the detection limit, showing no strong primary pollution. CO concentration was 0.22±0.07ppmv, and showed higher level during the start of the campaign (24 to 30 March), which could be resulted from the influence of BB (Fig 1d).

Although particles we measured in this study had larger size range than most of other studies, the results can still be comparable, considering that Aitken and accumulation mode particles, which all measurements included, constitute most of the particle number concentration (PN). Table 2 showed particle number concentrations in atmosphere at Mt. Yulong and other high altitude stations. Total number concentration of PM_{10} was 1600±1290 cm^{-3} during monsoon season of Mt. Yulong, slightly lower than those measured at other sites around Tibet Plateau, e.g. Waliguan and Mukteshwar, and Mt. Huang. However, this result is several times higher than those of areas with scarce emission sources, e.g. Alps and Antarctica. On the other hand, PN didn't show clear trend as the altitude increases, which means the regional emission and transport had larger impact on aerosols in upper troposphere, rather than the vertical distribution. We define N_{3-25}, N_{25-100}, $N_{100-1000}$, N_{1000+} as number concentrations of particles with

256   diameters of 3-25 nm, 25-100 nm, 100-1000 nm and 1-10 μm, respectively. There were

257   bursts of N_{3-25} on midday of 29 March, 4 April, 13 April, with the peak value at 9900

258   cm^{-3}, 11700 cm^{-3} and 5400 cm^{-3}, respectively (Fig.1c). During those periods, the

259   geometric mean diameter of the particles was lower than 25 nm. Those events could be

260   resulted from local or regional new particle formation, which would be discussed later.

261

262   3.1.2 Analysis of PNSD and PVSD

263   Average of PNSD during the measurement is showed in Fig.2a. In this study, we

264   sorted the particles by their sizes (Dal Maso et al., 2005). We consider that N_{25-100}

265   correlates to primary emission, and $N_{100-1000}$ has stronger connection with secondary

266   formation. According to results from bench tests and road tests, gasoline and diesel

267   vehicles will emit particles within 10–100 nm (Harris and Maricq, 2001;Kittelson et al.,

268   2006;Benajes et al., 2017;Tan et al., 2017). While studies on source apportionment of

269   atmospheric PNSD considered that the secondary formation or long range transport

270   mainly contributed particles within 100-1000 nm(Wang et al., 2013b;Vu et al., 2015).

271   The diameter with highest particle number concentration (D_{p-max}) was 107 nm. Number

272   concentration (dN/dlogDp) was larger than 1000 cm^{-3} between 40-200 nm, which was

273   the adjacent area of N_{25-100} and $N_{100-1000}$. This indicates that both primary emission

274   sources and secondary formation process had influences at Mt. Yulong site. N_{3-25}, N_{25-100},

275    $_{100}$, $N_{100-1000}$ were 244 cm^{-3}, 676 cm^{-3} and 638 cm^{-3}, constituting 16 %, 43 % and 41 %

276   of total concentration, respectively.

277   Different from PNSD, particle volume (PV) exhibited a bimodal distribution (Fig

278   2a). The first peak had an extreme value at 340 nm, representing the contribution of

279   primary emission and aging processes. This mass peak constituted 66 % of total PV,

280   including PV_{25-100} (2 %) and $PV_{100-1000}$ (64 %). 3-25 nm particles had negligible

281   influence on PV. Another mode in PV size distribution is within range of 1μm-10μm,

282   with the D_{p-max} at 2.2 μm. This mode could be attributed to the suspended soil. Volume

283   of 1-10μm particles constituted 34 % of total PV, similar with Qilian Shan station (38 %)

284 at Northeast Tibet Plateau (Xu et al., 2015), but higher than that urban Beijing (25 %)

285 (Wu et al., 2008), due to the much less emission sources and stronger wind at Mt.

286 Yulong.

287 To better characterize the contribution from different process, the mean PNSD was

288 fitted to three lognormal modes (Fig. 3, Table 3). We define the three fitted modes as

289 nucleation mode, Aitken mode and accumulation mode, based on their geometric mean

290 diameters, which were within 3-25 nm, 25-100 nm and 100-1000 nm, respectively.

291 Nucleation mode can be derived from nucleation process. Nucleation mode contributed

292 15 % to total PN, which was half lower than proportion of nucleation mode particles at

293 Mt. Tai, indicating relatively less impact from nucleation events. Median diameter of

294 Aitken mode and accumulation mode particles are 52 nm and 130 nm. These mean

295 diameters are similar with the results at Jungfraujoch (Bukowiecki et al., 2016) and

296 Beijing (Wu et al., 2008). Accumulation mode particles, correlating with secondary

297 formation (mode_3), contributed 54 % to total PN, which is twice higher than the result

298 in urban Beijing (Wu et al., 2008), and similar with that in pristine atmosphere of

299 Jungfraujoch (Bukowiecki et al., 2016). This result indicates that aerosols arrived at Mt.

300 Yulong were aged during the transport.

301

302 3.2 Influence of PBL diurnal variation on PNSD

303 Figure 4 shows the diurnal variation of N_{3-25}, N_{25-100}, $N_{100-1000}$ during the sampling

304 period. The particle number concentration in nucleation fraction and Aitken fraction

305 showed a clear diurnal variation. Mean value of N_{3-25} started to increase at 10:00 in the

306 morning, and reached around 500 cm^{-3} at noon due to nucleation events at noon (Fig.

307 4a). However, the median of N_{3-25} didn't showed similar diurnal variation because of

308 low NPF frequency. On the other hand, both mean and median of N_{25-100} showed a local

309 maximum during 10:00-14:00 (Fig. 4b). NPF events could not cause this variation,

310 since newly formed particles were not able to grow to 25 nm in the morning. So the

311 increased 25-100 nm particles originated from primary sources, e.g. traffic sources and

biomass burning. Considering that no anthropogenic emission sources around the site, those primary particles could be transported from other regions. During noon time, as the convection is strongest, N_{25-100} could be raised by the elevated urban PBL during the day, and anthropogenic particle injected during this process (Tröstl et al., 2016b). Adak et al. (2014) also reported that number concentration of PM_1 increased during day time, corresponding with the up-slope valley wind. In the afternoon, the convection become weaker, and the larger wind speed (Fig. 4e) had stronger scavenging effect on those primary particles, so N_{25-100} decreased at around 14:00.

The diurnal change of absolute water content also support that Mt. Yulong site was influenced by elevated PBL during midday. The water concentration was calculated based on temperature and relative humidity, and showed an increase from 3.3 g m^{-1} to 4.2 g m^{-1} during 9:00-12:00, and descended back to 3.6 g m^{-1} till 14:00 (Fig. 4f). This systematic water content variation indicates that the site was influenced by the PBL during day time. Shen et al (2016) used the increase of water content together with Aitken mode particles, to separate the PBL conditions at Mt. Tai. The value of CO/NO_y and NO_y/NO_x was used in other studies to determine the age of the air masses arriving high altitude sites (Tröstl et al., 2016b;Zellweger et al., 2003;Jaeglé et al., 1998). Because NO_y was not measured in this study, we used CO/NO_x to estimate the age of air mass since contact with primary emission. CO/NO_x was 287 ± 146 at Mt. Yulong, lower than Jungfraujoch (Herrmann et al., 2015), Mt. Cimone (Cristofanelli et al., 2016) and Kansas (Jaeglé et al., 1998), indicating a stronger anthropogenic influence. The diurnal variation of CO/NO_x showed minimum during 9:00-14:00 (Fig. 4d), consistent with the local maximum of water content and N_{25-100}. The diurnal variation of O_3/NO_x exhibited a similar trend as CO/NO_x, with an average of 69.6 during 10:00-14:00, and 83.6 during 1:00-6:00 (Fig. S2). Those evidences indicate that at least during 10:00-14:00, Mt. Yulong site was influenced by elevated PBL. On the other hand, we consider the data during 1:00-6:00 as the condition within FT, when N_{25-100} and water content were lowest and CO/NO_x were highest. However, $N_{100-1000}$ didn't show obvious diurnal variation, indicating the elevated PBL didn't inject large amount of 100-1000 nm particles.

342 3.3 Influences of BB on Mt. Yulong

343 3.3.1 Identification of BB episodes

344   Background condition (BG) was picked during 1 to 4 April, when the
345 concentration of BC was 85 ng m^{-3} on average. During this period, the wind was
346 relatively stronger, and fire spots were barely found on the westward path of the air
347 mass (Fig. S3). Based on the background condition, three BB events were identified by
348 the following criteria: 1) BC was more than the background level (85 ng m^{-3}); 2) higher
349 fraction of f60 than during BG (0.4 %); 3) fire spots appeared in the source regions of
350 the air masses or surrounding areas of the site.

351   During the first BB event (BB1, 22 to 30 March), dense fire spots were found on
352 the source region in north Burma. BC concentration (1.2 μg m^{-3}), PV and f60 signal
353 showed highest level during BB1. Trajectories of BB2 (5 to 6 April) passed fewer fire
354 spots in South Asia than BB1, and the BC concentration was lower (0.3 μg m^{-3}).
355 Concentration of organic components during BB2 was 4 times as that during
356 background period. According to an AMS study from the same campaign, organic
357 particles during BB2 were mainly influenced by transported oxidized organics
358 originated from biomass burning (OOA-BB), other than fresh BB organic aerosols
359 (Zheng et al., 2017). The proportion of f60 was highest (1.4 %) during BB3 (11 to 12
360 April), showing strong BB influence. However, few fire spots were observed on the
361 path of air mass, indicating the BB particles could be derived from domestic heating
362 nearby. Zheng's study (2017) also indicated that organic aerosols showed character
363 closer with fresh BBOA compared with BB1.

364 3.3.2 Influences of BB on PNSD and CCN

365   The average PNSDs during BB events and BG condition were plotted in Figure 5,
366 and fitted by 3-mode lognormal distributions. The fitting results are showed in Table 3.
367 For the BG condition, only two modes were obtained (Fig. 5d), including nucleation
368 mode (mode_1, D$_{mean}$ = 15 nm) originated from nucleation events and Aitken mode

369   (mode_2, D_{mean} = 79 nm). Their total number concentration was 669 cm^{-3}, similar with

370   the level at Swiss Jungfraujoch (Herrmann et al., 2015), exhibiting an Eurasia

371   background character.

372   The averaged PNSD during those BB episodes showed discrepancies, indicating

373   the variant influences of transported and local BB on particles in atmosphere of Mt.

374   Yulong. During the BB2, Aitken mode number concentration was similar with that

375   during BG condition. But an accumulation mode (mode_3, D_{mean} = 106 nm) with higher

376   PN (775 cm^{-3}) appeared (Fig. 5b). This mode with larger size could be the aged particles

377   transported from BB source regions in South Asia. Different from BB2, Aitken mode

378   particles were increased by a factor of 3 and became dominant in PNSD during BB3

379   the local event (Fig. 5c). The number concentration of this mode was 1309 cm^{-3}, 2 times

380   more than accumulation mode particles. The reason could be that the particles during

381   BB3 were freshly emitted from sources nearby the monitoring site. The study of Zheng

382   et al (2017) also showed that during this period, the OOA fraction in organic aerosols

383   was relatively lower, while BBOA fraction was higher, indicating impacts from more

384   local BB sources. The geometric mean diameters of accumulation mode were 169, 106,

385   130 nm during BB1, BB2, and BB3, smaller than that of aged biomass burning particles

386   at Mt. Bachelor, USA (Laing et al., 2016), indicating the particles at Mt. Yulong were

387   more fresh. Nucleation mode had lower PN during BB2 and BB3, since the higher PN

388   of larger particles played as strong coagulation sink of nucleation mode particles.

389   Aitken mode and accumulation mode were comparable during BB1 (Fig. 5a), indicating

390   the fresh aerosols from sources surrounding the site had comparable influence as the

391   transported aged BB aerosols.

392   In a word, the BG condition at Mt. Yulong could represent the background level

393   of particles of TP or even Eurasia. The local and long-range transported BB emissions

394   would increase the level of Aitken mode and accumulation mode particles, respectively.

395

396   Concentration of CCN was calculated following method described in section 2.3.3.

397   κ value during the sampling period was 0.12±0.01, only 1/3 from urban Beijing (Wu et

398   al., 2016) and a rural site at Thuringia, Germany (Wu et al., 2013), but consistent with

399   the results in Alberta, Canada (0.11±0.04) during BB events (Lathem et al., 2013).

400   Pierce et al (2012) reported that κ was around 0.1 for >100 nm particles in a forest

401   mountain valley during biogenic secondary organic aerosols formation and growth

402   events. Similarly, organic volume fraction was 0.73 in particle at Mt. Yulong,

403   explaining the low value of κ. As a result, the D_c at SS of 0.6 % and 1.2 % was 72.0±2.2

404   and 45.4±1.4 nm, respectively. There could be uncertainties for value of κ and D_c, since

405   here we used a manually set hygroscopicity of organics, which may varied with

406   oxidation level or other factors (Wu et al., 2016). Considering the variation range of D_c

407   was small, the CCN concentration was mainly controlled by size distribution of particle

408   number.

409   BB events raised the CCN level in atmosphere by influencing the PNSD. Increase

410   of PN was observed during BB events, i.e. 2207±1388 cm^{-3}, 1214±638 cm^{-3},

411   2062±1112 cm^{-3} during BB1, BB2, BB3, respectively. As a consequence, the increased

412   particles played as CCN in atmosphere of Mt. Yulong, forming a readily increase of

413   CCN concentration during BB events. Figure 6 showed the mean number concentration

414   of CCN in periods under PBL influence (10:00-14:00, as discussed in 3.2) and FT

415   condition (1:00-6:00) during BG and BB events. Mean number concentration of CCN

416   under supersaturation of 0.6 % was 936±754 cm^{-3} and 807±705 cm^{-3} for PBL and FT

417   periods at Mt. Yulong, comparative with boreal forest station in Finland (Cerully et al.,

418   2011). The concentration of CCN in PBL condition during BB1, BB2, BB3 was 5, 2, 2

419   times as that during BG. Promotions of CCN during BB1, BB2, BB3 were more

420   remarkable for FT, i.e. 9, 3, 8 times as BG (Fig. 6). This result indicates that the BB

421   particles from South Asia could have strong influence on the climate parameter. For the

422   data under supersaturation of 1.2 %, the ratios between CCN concentration of BBs and

423   that of BG were less, i.e. 2-4 times for periods influenced by PBL, and 2-7 times for FT

424   conditions. This is because critical diameters under supersaturation 0.6 % and 1.2 %

425   were around 72 nm and 45 nm, respectively. And PN within 45-72 nm was relatively

426   stable compared to the larger particles, because of the daily input of anthropogenic

427   primary aerosols from urban air masses.

428 3.4 New particle formation events

429 3.4.1 NPF events at Mt. Yulong under anthropogenic influences

430   Following the method Tröstl et al (2016b) and Yli-Juuti et al (2009) used, we
431 define the three NPF events on 29 March, 4 and 13 April as follows:

432 a) Type A event on 29 March: appearance of newly formed particles (3 nm, the first
433   bin of nano-SMPS) and continuous growth of those particles, reaching the upper
434   limit of nucleation mode (25 nm). This NPF event was within the period of BB1,
435   the air mass arriving at Mt. Yulong was from North part of Burma with slow
436   movement before 28 March, transporting abundant pollutants to this area. During
437   28 March 12:00 to 29 March 6:00, the air mass was from west upper troposphere
438   (Fig S4), cleaning out the pre-existing particles built up by BB events. CS at Mt.
439   Yulong decreased from 0.006 s^{-1} to 0.002 s^{-1} on morning of 29 March. On the other
440   hand, the concentration of SO_2 was stable (around 0.04 ppb) before occurrence of
441   nucleation. The calculated H_2SO_4 increased before nucleation, reaching 5×10^6 cm^{-}
442   ^{3} (Fig. S4). The nucleation rate was 1.43 cm^{-3}s^{-1}, increasing nucleation mode
443   particles to around 10^4 cm^{-3}. Benefited by the increase of α-pinene (from 0.02 ppb
444   to 0.10 ppb), β-pinene (from 0.03 ppb to 0.20 ppb) and SO_2 in day of 29 March, the
445   formation of secondary aerosol continued, and the newly formed particles grew
446   over 30 nm before night. This process could be from gaseous oxidation and
447   condensation. Particle growth stopped during night of 29 March, when the gaseous
448   reaction was inhibited because of absence of sunlight. After sunrise on 30 March,
449   the particle continued growing and reached 40 nm. Concentration of toluene was
450   lower than 0.1 ppb, indicating small contribution from anthropogenic VOCs. The
451   GR was 3.48 nm h^{-1} within size range of 3-25 nm. In a word, under the influence of
452   transported pollutants, nucleation was triggered by the upper clean air mass, which
453   reduced level of pre-existing particles. While growth of particles was favored by
454   the photochemical reaction and condensation process.

455

456   b) Type B event on 4 April: newly formed mode occurred with growing trend, but

457   growth stopped at early stage (<15 nm), and there were temporal low values of N_{3-}

458       $_{25}$ during the event. The event on 4 April was under BG condition, during which

459   concentration of SO_2 was lower (around 0.02 ppb). Started from 2:00 on 4 April,

460   the air mass arrived at Mt. Yulong was transported by upslope flow from west lower

461   troposphere. While during 9:00-12:00, the air mass arrived at Mt. Yulong passed

462   Northeast India, where fire spots could be observed on the MODIS map during 2

463   April. Thus, the gaseous pollutants and particles from anthropogenic sources nearby

464   or from BB sources in Northeast India was transported to this site on morning of 4

465   April. Concentration of SO_2 and $[H_2SO_4]$ increased to 0.07 ppb and 6×10^6 cm^{-3} at

466   11:00, respectively, corresponding to occurrence nucleation (Fig. S5). SO_2 shared

467   similar time series with black carbon, indicating a combustion source. FR and GR

468   were 0.93 cm^{-3} s^{-1} and 3.2 nm h^{-1}, respectively. N_{3-25} fluctuated during NPF events,

469   showing low values when there were temporary changes in cloud condition

470   (influencing radiation) and wind direction. Concentrations of β-pinene and Toluene

471   were stable and lower than 0.10 ppb and 0.65 ppb respectively throughout the NPF

472   event, which could be the reason of smaller growth rate. At around 14:00, the source

473   region of air mass varied to west upper troposphere, and the stronger wind cleaned

474   out both the nucleated mode particles and gaseous precursors, terminating the NPF

475   event. In summary, type B event under background condition was triggered by the

476   injection of gaseous pollutants from elevated PBL and short term transport of BB

477   pollutants.

478

479   c) Off-site NPF event on 13 April: A narrow band (8-50 nm) was observed in PNSD

480   from 13 to 14 April. The primary particles should have wider range and larger size.

481   These particles were mostly likely nucleated off-site, and transported to Mt. Yulong

482   site by uplifting air mass. On the afternoon of 13 April, the air mass arrived at Mt.

483   Yulong passed the local ground layer (yellow trajectory in Fig S6). SO_2 increased

484   from 0.06 ppb to 0.13 ppb, and toluene reached highest level at 0.098 ppb (Fig. S6),

485   indicating an anthropogenic impact. As a result, particles formed from the ground

486   level were transported to the site and a burst of N_{3-25} occurred at around 18:00. β-

487   pinene also showed higher value at dawn of 13 April. Those nanoparticles showed

488   a growth trend, with GR at 2.99 nm h^{-1}. To summarize, occurrence of nucleation

489   mode particles were off-site nucleated in PBL and transported to this site.

490

491   The new particle formation events had strong influences on PNSD. Particles

492   showed unimodal distribution during non-NPF event periods, with the peak diameter at

493   around 125 nm (Fig 7S). This is mainly due to the impact from aged biomass burning

494   particles. During those NPF events, PNSD showed a clear bimodal characteristic. The

495   smaller mode was originated from nucleation and growth of nanoparticles. This mode

496   had a higher peak than the larger mode, indicating that NPF significantly contributed

497   to particle number concentration.

498   3.4.2 Limiting factors of NPF events

499   Frequency of NPF was 14 % during our measurement. This NPF frequency is

500   clearly less than polluted atmosphere of North China Plain (40-65 %) in March and

501   April (Wang et al., 2013a;Shen et al., 2011), the top of Mt. Huang (38 %) during April

502   (Zhang et al., 2016), a background site in Northeast Tibet Plateau (79%) in autumn (Du

503   et al., 2015) and a remote rural site in the Sierra Nevada Mountains (47 %) in spring

504   (Creamean et al., 2011). A common knowledge is that CS is the limiting factor that

505   controls the NPF (Cai et al., 2017). Thus, pre-existing particle levels on event days

506   should be less than non-event days, at high altitude mountain sites (Shen et al.,

507   2016;Guo et al., 2012) as well as urban sites (Wang et al., 2011;Wang et al., 2017). The

508   low NPF frequency was unexpected in clean atmosphere of Mt. Yulong, since the mean

509   CS at Mt. Yulong was 0.0038 s^{-1}. On the other hand, similar low frequency of NPF

510   events were also observed in pristine atmospheres, e.g. 24 % at Antarctic site Neumayer

511   (Weller et al., 2015), 12-17 % at Dome C, Antarctica (Järvinen et al., 2013).

512   During the first five days of the campaign (22 to 27 March), the nucleation events

513   could be prevented by large amount of pre-existing particles acting as big condensation

514   sink. The CS was more than 0.005 s^{-1}, similar with polluted Beijing on days with NPF

515   events (Wu et al., 2007). However, on rest of days when CS was even lower than 0.002

516   s^{-1}, the NPF events were still scarce. Considering that the content of condensable vapor

517   participated in nucleation is determined by the competition between formation from

518   precursor oxidation and condensation on surface of pre-existing particles (Zhang et al.,

519   2012), the lower NPF frequency at pristine sites could be resulted from lack of precursor,

520   e.g. VOCs and SO$_2$ from fossil fuel and biomass burning sources.

521   To further evaluate the effect of different parameters on NPF, daily variations of

522   SO$_2$, CS, J(O^{1}D), Benzene and β-pinene during 28 March to 14 April were calculated

523   and plotted in Figure 7. The results during 10:00-14:00 were picked up as the

524   occurrence time of nucleation, and compared between NPF days and non-event days.

525   As shown in Fig. 7, NPF days and non-NPF days shared same level of J(O^{1}D), and 15 %

526   difference in CS when nucleation happened, indicating small influence of solar

527   radiation and pre-existing particles on NPF. In addition to this, if we took out the data

528   under biomass burning influences from non-NPF days, the averaged PNSD (Fig S7)

529   was similar with the PNSD during NPF days in larger size range (> 80 nm). Considering

530   that larger particles are the main contributor to condensation and coagulation sink, we

531   can conclude that in the pristine atmosphere of Mt. Yulong, CS is not the decisive factor

532   on NPF.

533   The concentration of SO$_2$ showed increase on NPF days, 60 % higher than non-

534   event days, indicating the anthropogenic SO$_2$ as the controlling factor of NPF at Mt.

535   Yulong. Studies at Jungfraujoch (Bianchi et al., 2016;Tröstl et al., 2016b), Izaña (García

536   et al., 2014) and Mukteshwar (Neitola et al., 2011) also reported that the nucleation

537   events in upper troposphere corresponded to increase of anthropogenic gas pollutants

538   by elevated PBL. At Daban Mountain on the North slope of TP, the PM$_{2.5}$ level was

539   similar with Mt. Yulong, but NPF could be observed nearly every day. It may be caused

540   by that the SO$_2$ was around 2 ppb on average, two order of magnitude higher than Mt.

541   Yulong.

542   Organics may also be a driven factor on NPF. The concentration of β-pinene

543   showed higher value (40 %) in the afternoon on NPF days, while there was little

difference (9 %) between NPF days and non-event days on anthropogenic benzene. Recent studies considered that apart from sulfuric acid, the highly oxidized multifunctional organics from biogenic VOCs could take part in nucleation as well as growth (Huang et al., 2016;Tröstl et al., 2016a), in free troposphere, the pure organic nucleation without sulfuric acid may even be dominant (Bianchi et al., 2016;Gordon et al., 2016). According to Du et al 's study(2015), the fraction of oxidized organics in particle phase had positive relationship with particle growth rate, indicating the contribution from organics to particle growth. So the increase of biogenic VOCs could benefit the nucleation and growth of nucleation mode particles at Mt. Yulong.

3.4.3 Parameters of NPF events in this study

Formation rate, growth rate and condensation sink of NPF events at Mt. Yulong were summarized in Table 4. Compared with other high mountain measurements, this study reported a higher FR, e.g. 3 times as that at Storm peak laboratory (Hallar et al., 2011). But the GR at Mt. Yulong was within average level, indicating different precursors participating in nucleation and growth process. Even though SO_2 was well correlated with nucleation events, the calculated growth rate by condensation of H_2SO_4 can only explain 5 % of the measured GR. This result indicated participation of some other precursors in particle growth, e.g. organics.

4. Conclusion

PNSD, meteorological parameters, trace gases and particle chemical composition were measured at Mt. Yulong site (3410 m a.s.l.) in Southeast corner of Tibet Plateau, during pre-monsoon season (22 March to 15 April) of 2015. PNSD in background atmosphere of Tibet Plateau was characterized. As a background site in Southwest China, the atmosphere of Mt. Yulong exhibited lower particle level and stronger oxidation capacity than low attitude atmosphere.

PBL convection is an influencing factor of PNSD, which caused readable diurnal

572 variation of N_{ait}. Diurnal variation of CO/NO_x and absolute humidity showed that the

573 monitoring site was influenced by PBL during 10:00-14:00, and showed typical FT

574 condition during 1:00-6:00.

575 Three different types of BB event periods were identified by content of BC, $f60$,

576 air mass backward trajectory and fire spot map. Accumulation mode was dominant in

577 transported BB particles from Myanmar, but less aged compared with other Tibet

578 Plateau sites under influence of BB. Under local biomass burning episode, Aitken mode

579 was dominant in PNSD. The biomass burning from South Asia had strong influence on

580 climate parameters, especially for FT. Concentrations of CCN in FT at Mt. Yulong

581 during BB events were 3-9 times as that during BG period. Due to high fraction of

582 organic compounds, the CCN activity of particles in atmosphere of Mt. Yulong was

583 lower than other high altitude sites and ground level sites.

584 Unexpected low NPF frequency was found in clean atmosphere at Mt. Yulong,

585 due to low concentration of anthropogenic precursor, i.e. SO_2. Occurrence of NPF

586 events were favored by elevated surface emission of SO_2 and transported BB pollutants

587 from South Asia. Off-site NPF event was also observed, during which nanoparticles

588 were formed in PBL and transported to the site. Condensation of sulfuric acid can only

589 explain 5 % of GR in on-site NPF events, indicating other precursors participating in

590 particle growth. NPF can hardly contribute to CCN, since the newly formed particles

591 cannot reach the critical diameter.

592 Our study provided important dataset of particle physical properties at Tibet

593 Plateau. Influences of BB activities in South Asia and local area on PNSD and CCN in

594 atmosphere of Tibet Plateau were highlighted. Different types of NPF in upper

595 troposphere in Southwest China were characterized, and role of SO_2 were analyzed.

596 Results of our study could be used in regional and global climate model, and help

597 building up the knowledge of NPF in upper part of troposphere.

598

599 **Acknowledgement**

600 This study was supported by National Natural Science Foundation of China (91544214,

601 51636003, 21677002), the China Ministry of Environmental Protection Special Funds

for Scientific Research on Public Welfare (201309016). We thank Jie Li and Zhangyu Qia from for help with running the WRF model. We also thank the colleagues in the China National Environmental Monitoring Center and Lijiang Monitoring Station for the support to the field campaign.

References

Adak, A.: Atmospheric Fine Mode Particulates at Eastern Himalaya, India: Role of Meteorology, Long-Range Transport and Local Anthropogenic Sources, Aerosol and Air Quality Research, 10.4209/aaqr.2013.03.0090, 2014.

Benajes, J., Garcia, A., Monsalve-Serrano, J., and Boronat, V.: Gaseous emissions and particle size distribution of dual-mode dual-fuel diesel-gasoline concept from low to full load, Applied Thermal Engineering, 120, 138-149, 2017.

Bianchi, F., Tröstl, J., Junninen, H., Frege, C., Henne, S., Hoyle, C. R., Molteni, U., Herrmann, E., Adamov, A., Bukowiecki, N., Chen, X., Duplissy, J., Gysel, M., Hutterli, M., Kangasluoma, J., Kontkanen, J., Kürten, A., Manninen, H. E., Münch, S., Peräkylä, O., Petäjä, T., Rondo, L., Williamson, C., Weingartner, E., Curtius, J., Worsnop, D. R., Kulmala, M., Dommen, J., and Baltensperger, U.: New particle formation in the free troposphere: A question of chemistry and timing, Science, 352, 1109, 2016.

Bonasoni, P., Laj, P., Marinoni, A., Sprenger, M., Angelini, F., Arduini, J., Bonafè, U., Calzolari, F., Colombo, T., Decesari, S., Di Biagio, C., di Sarra, A. G., Evangelisti, F., Duchi, R., Facchini, M. C., Fuzzi, S., Gobbi, G. P., Maione, M., Panday, A., Roccato, F., Sellegri, K., Venzac, H., Verza, G. P., Villani, P., Vuillermoz, E., and Cristofanelli, P.: Atmospheric Brown Clouds in the Himalayas: first two years of continuous observations at the Nepal Climate Observatory-Pyramid (5079 m), Atmos. Chem. Phys., 10, 7515-7531, 10.5194/acp-10-7515-2010, 2010.

Boy, M., Karl, T., Turnipseed, A., Mauldin, R. L., Kosciuch, E., Greenberg, J., Rathbone, J., Smith, J., Held, A., Barsanti, K., Wehner, B., Bauer, S., Wiedensohler, A., Bonn, B., Kulmala, M., and Guenther, A.: New particle formation in the Front Range of the Colorado Rocky Mountains, Atmos. Chem. Phys., 8, 1577-1590, 10.5194/acp-8-1577-2008, 2008.

Bukowiecki, N., Weingartner, E., Gysel, M., Coen, M. C., Zieger, P., Herrmann, E., Steinbacher, M., Gäggeler, H. W., and Baltensperger, U.: A Review of More than 20 Years of Aerosol Observation at the High Altitude Research Station Jungfraujoch, Switzerland (3580 m asl), Aerosol and Air Quality Research, 16, 764-788, 10.4209/aaqr.2015.05.0305, 2016.

Cai, R., Yang, D., Fu, Y., Wang, X., Li, X., Ma, Y., Hao, J., Zheng, J., and Jiang, J.: Aerosol Surface Area Concentration: a Governing Factor for New Particle Formation in Beijing, Atmos. Chem. Phys. Discuss., 2017, 1-26, 10.5194/acp-2017-467, 2017.

Cerully, K. M., Raatikainen, T., Lance, S., Tkacik, D., Tiitta, P., Petäjä, T., Ehn, M., Kulmala, M., Worsnop, D. R., Laaksonen, A., Smith, J. N., and Nenes, A.: Aerosol hygroscopicity and CCN activation kinetics in a boreal forest environment during the 2007 EUCAARI campaign, Atmospheric Chemistry and Physics, 11, 12369-12386, 10.5194/acp-11-12369-2011, 2011.

Chen, Y., Cao, J., Zhao, J., Xu, H., Arimoto, R., Wang, G., Han, Y., Shen, Z., and Li, G.: N-alkanes and polycyclic aromatic hydrocarbons in total suspended particulates from the southeastern Tibetan Plateau: concentrations, seasonal variations, and sources, The Science of the total environment, 470-471, 9-18,

643 10.1016/j.scitotenv.2013.09.033, 2014.

644 Cong, Z., Kang, S., Kawamura, K., Liu, B., Wan, X., Wang, Z., Gao, S., and Fu, P.: Carbonaceous aerosols

645 on the south edge of the Tibetan Plateau: concentrations, seasonality and sources, Atmos. Chem. Phys.,

646 15, 1573-1584, 10.5194/acp-15-1573-2015, 2015.

647 Creamean, J. M., Ault, A. P., Ten Hoeve, J. E., Jacobson, M. Z., Roberts, G. C., and Prather, K. A.:

648 Measurements of aerosol chemistry during new particle formation events at a remote rural mountain

649 site, Environmental science & technology, 45, 8208-8216, 10.1021/es103692f, 2011.

650 Cristofanelli, P., Landi, T. C., Calzolari, F., Duchi, R., Marinoni, A., Rinaldi, M., and Bonasoni, P.: Summer

651 atmospheric composition over the Mediterranean basin: Investigation on transport processes and

652 pollutant export to the free troposphere by observations at the WMO/GAW Mt. Cimone global station

653 (Italy, 2165 m a.s.l.), Atmospheric Environment, 141, 139-152, 10.1016/j.atmosenv.2016.06.048, 2016.

654 D'Andrea, S. D., Ng, J. Y., Kodros, J. K., Atwood, S. A., Wheeler, M. J., Macdonald, A. M., Leaitch, W. R.,

655 and Pierce, J. R.: Source attribution of aerosol size distributions and model evaluation using Whistler

656 Mountain measurements and GEOS-Chem-TOMAS simulations, Atmos. Chem. Phys., 16, 383-396,

657 10.5194/acp-16-383-2016, 2016.

658 Dal Maso, M., Kulmala, M., Riipinen, I., Wagner, R., Hussein, T., Aalto, P. P., and Lehtinen, K. E. J.:

659 Formation and growth of fresh atmospheric aerosols: eight years of aerosol size distribution data from

660 SMEAR II, Hyytiala, Finland, Boreal Environ. Res., 10, 323-336, 2005.

661 Draxier, R. R., and Hess, G. D.: An overview of the HYSPLIT_4 modelling system for trajectories,

662 dispersion and deposition, Aust. Meteorol. Mag., 47, 295-308, 1998.

663 Du, W., Sun, Y. L., Xu, Y. S., Jiang, Q., Wang, Q. Q., Yang, W., Wang, F., Bai, Z. P., Zhao, X. D., and Yang, Y.

664 C.: Chemical characterization of submicron aerosol and particle growth events at a national background

665 site (3295 m a.s.l.) on the Tibetan Plateau, Atmos. Chem. Phys., 15, 10811-10824, 10.5194/acp-15-

666 10811-2015, 2015.

667 Ehhalt, D. H., and Rohrer, F.: Dependence of the OH concentration on solar UV, J Geophys Res-Atmos,

668 105, 3565-3571, 10.1029/1999jd901070, 2000.

669 Fröhlich, R., Cubison, M. J., Slowik, J. G., Bukowiecki, N., Canonaco, F., Croteau, P. L., Gysel, M., Henne,

670 S., Herrmann, E., Jayne, J. T., Steinbacher, M., Worsnop, D. R., Baltensperger, U., and Prévôt, A. S. H.:

671 Fourteen months of on-line measurements of the non-refractory submicron aerosol at the Jungfraujoch

672 (3580 m a.s.l.) – chemical composition, origins and organic aerosol sources, Atmos. Chem. Phys., 15,

673 11373-11398, 10.5194/acp-15-11373-2015, 2015.

674 García, M. I., Rodríguez, S., González, Y., and García, R. D.: Climatology of new particle formation at Izaña

675 mountain GAW observatory in the subtropical North Atlantic, Atmos. Chem. Phys., 14, 3865-3881,

676 10.5194/acp-14-3865-2014, 2014.

677 Gautam, R., Hsu, N. C., Lau, K. M., Tsay, S. C., and Kafatos, M.: Enhanced pre-monsoon warming over

678 the Himalayan-Gangetic region from 1979 to 2007, Geophysical Research Letters, 36, n/a-n/a,

679 10.1029/2009gl037641, 2009.

680 Gordon, H., Sengupta, K., Rap, A., Duplissy, J., Frege, C., Williamson, C., Heinritzi, M., Simon, M., Yan, C.,

681 Almeida, J., Trostl, J., Nieminen, T., Ortega, I. K., Wagner, R., Dunne, E. M., Adamov, A., Amorim, A.,

682 Bernhammer, A. K., Bianchi, F., Breitenlechner, M., Brilke, S., Chen, X. M., Craven, J. S., Dias, A., Ehrhart,

683 S., Fischer, L., Flagan, R. C., Franchin, A., Fuchs, C., Guida, R., Hakala, J., Hoyle, C. R., Jokinen, T., Junninen,

684 H., Kangasluoma, J., Kim, J., Kirkby, J., Krapf, M., Kurten, A., Laaksonen, A., Lehtipalo, K., Makhmutov, V.,

685 Mathot, S., Molteni, U., Monks, S. A., Onnela, A., Perakyla, O., Piel, F., Petaja, T., Praplanh, A. P., Pringle,

686 K. J., Richards, N. A. D., Rissanen, M. P., Rondo, L., Sarnela, N., Schobesberger, S., Scott, C. E., Seinfeldo,

J. H., Sharma, S., Sipila, M., Steiner, G., Stozhkov, Y., Stratmann, F., Tome, A., Virtanen, A., Vogel, A. L., Wagner, A. C., Wagner, P. E., Weingartner, E., Wimmer, D., Winkler, P. M., Ye, P. L., Zhang, X., Hansel, A., Dommen, J., Donahue, N. M., Worsnop, D. R., Baltensperger, U., Kulmala, M., Curtius, J., and Carslaw, K. S.: Reduced anthropogenic aerosol radiative forcing caused by biogenic new particle formation, Proceedings of the National Academy of Sciences of the United States of America, 113, 12053-12058, 10.1073/pnas.1602360113, 2016.

Guo, H., Wang, D. W., Cheung, K., Ling, Z. H., Chan, C. K., and Yao, X. H.: Observation of aerosol size distribution and new particle formation at a mountain site in subtropical Hong Kong, Atmospheric Chemistry and Physics, 12, 9923-9939, 10.5194/acp-12-9923-2012, 2012.

Gysel, M., Crosier, J., Topping, D. O., Whitehead, J. D., Bower, K. N., Cubison, M. J., Williams, P. I., Flynn, M. J., McFiggans, G. B., and Coe, H.: Closure study between chemical composition and hygroscopic growth of aerosol particles during TORCH2, Atmos. Chem. Phys., 7, 6131-6144, 10.5194/acp-7-6131-2007, 2007.

Hallar, A. G., Lowenthal, D. H., Chirokova, G., Borys, R. D., and Wiedinmyer, C.: Persistent daily new particle formation at a mountain-top location, Atmospheric Environment, 45, 4111-4115, 10.1016/j.atmosenv.2011.04.044, 2011.

Harris, S., and Maricq, M. M.: Signature size distributions for diesel and gasoline engine exhaust particulate matter, 749-764 pp., 2001.

Herrmann, E., Weingartner, E., Henne, S., Vuilleumier, L., Bukowiecki, N., Steinbacher, M., Conen, F., Collaud Coen, M., Hammer, E., Jurányi, Z., Baltensperger, U., and Gysel, M.: Analysis of long-term aerosol size distribution data from Jungfraujoch with emphasis on free tropospheric conditions, cloud influence, and air mass transport, Journal of Geophysical Research: Atmospheres, 120, 9459-9480, 10.1002/2015jd023660, 2015.

Huang, X., Zhou, L., Ding, A., Qi, X., Nie, W., Wang, M., Chi, X., Petäjä, T., Kerminen, V. M., Roldin, P., Rusanen, A., Kulmala, M., and Boy, M.: Comprehensive modelling study on observed new particle formation at the SORPES station in Nanjing, China, Atmos. Chem. Phys., 16, 2477-2492, 10.5194/acp-16-2477-2016, 2016.

Hussein, T., Dal Maso, M., Petaja, T., Koponen, I. K., Paatero, P., Aalto, P. P., Hameri, K., and Kulmala, M.: Evaluation of an automatic algorithm for fitting the particle number size distributions, Boreal Environ. Res., 10, 337-355, 2005.

Järvinen, E., Virkkula, A., Nieminen, T., Aalto, P. P., Asmi, E., Lanconelli, C., Busetto, M., Lupi, A., Schioppo, R., Vitale, V., Mazzola, M., Petäjä, T., Kerminen, V. M., and Kulmala, M.: Seasonal cycle and modal structure of particle number size distribution at Dome C, Antarctica, Atmospheric Chemistry and Physics, 13, 7473-7487, 10.5194/acp-13-7473-2013, 2013.

Jaeglé, L., Jacob, D. J., Wang, Y., Weinheimer, A. J., Ridley, B. A., Campos, T. L., Sachse, G. W., and Hagen, D. E.: Sources and chemistry of NOxin the upper troposphere over the United States, Geophysical Research Letters, 25, 1705-1708, 10.1029/97gl03591, 1998.

Kittelson, D. B., Watts, W. F., and Johnson, J. P.: On-road and laboratory evaluation of combustion aerosols—Part1: Summary of diesel engine results, Journal of Aerosol Science, 37, 913-930, https://doi.org/10.1016/j.jaerosci.2005.08.005, 2006.

Kivekäs, N., Sun, J., Zhan, M., Kerminen, V. M., Hyvärinen, A., Komppula, M., Viisanen, Y., Hong, N., Zhang, Y., Kulmala, M., Zhang, X. C., Deli, G., and Lihavainen, H.: Long term particle size distribution measurements at Mount Waliguan, a high-altitude site in inland China, Atmos. Chem. Phys., 9, 5461-5474, 10.5194/acp-9-5461-2009, 2009.

Komppula, M., Lihavainen, H., Hyvärinen, A. P., Kerminen, V. M., Panwar, T. S., Sharma, V. P., and Viisanen, Y.: Physical properties of aerosol particles at a Himalayan background site in India, Journal of Geophysical Research, 114, 10.1029/2008jd011007, 2009.

Kulmala, M., maso, M. D., Mäkelä, J. M., Pirjola, L., Väkevä, M., Aalto, P., Miikkulainen, P., Hämeri, K., #039, and dowd, C. D.: On the formation, growth and composition of nucleation mode particles, 2001, 53, 10.3402/tellusb.v53i4.16622, 2001.

Lüthi, Z. L., Škerlak, B., Kim, S. W., Lauer, A., Mues, A., Rupakheti, M., and Kang, S.: Atmospheric brown clouds reach the Tibetan Plateau by crossing the Himalayas, Atmos. Chem. Phys., 15, 6007-6021, 10.5194/acp-15-6007-2015, 2015.

Laing, J. R., Jaffe, D. A., and Hee, J. R.: Physical and optical properties of aged biomass burning aerosol from wildfires in Siberia and the Western USA at the Mt. Bachelor Observatory, Atmos. Chem. Phys., 16, 15185-15197, 10.5194/acp-16-15185-2016, 2016.

Lathem, T. L., Beyersdorf, A. J., Thornhill, K. L., Winstead, E. L., Cubison, M. J., Hecobian, A., Jimenez, J. L., Weber, R. J., Anderson, B. E., and Nenes, A.: Analysis of CCN activity of Arctic aerosol and Canadian biomass burning during summer 2008, Atmospheric Chemistry and Physics, 13, 2735-2756, 10.5194/acp-13-2735-2013, 2013.

Lunden, M. M., Black, D. R., McKay, M., Revzan, K. L., Goldstein, A. H., and Brown, N. J.: Characteristics of Fine Particle Growth Events Observed Above a Forested Ecosystem in the Sierra Nevada Mountains of California, Aerosol Science and Technology, 40, 373-388, 10.1080/02786820600631896, 2006.

Merikanto, J., Spracklen, D. V., Mann, G. W., Pickering, S. J., and Carslaw, K. S.: Impact of nucleation on global CCN, Atmospheric Chemistry And Physics, 9, 8601-8616, 10.5194/acp-9-8601-2009, 2009.

Neitola, K., Asmi, E., Komppula, M., Hyvärinen, A. P., Raatikainen, T., Panwar, T. S., Sharma, V. P., and Lihavainen, H.: New particle formation infrequently observed in Himalayan foothills – why?, Atmospheric Chemistry and Physics, 11, 8447-8458, 10.5194/acp-11-8447-2011, 2011.

Nishita, C., Osada, K., Kido, M., Matsunaga, K., and Iwasaka, Y.: Nucleation mode particles in upslope valley winds at Mount Norikura, Japan: Implications for the vertical extent of new particle formation events in the lower troposphere, Journal of Geophysical Research, 113, 10.1029/2007jd009302, 2008.

Okamoto, S., and Tanimoto, H.: A review of atmospheric chemistry observations at mountain sites, Progress in Earth and Planetary Science, 3, 10.1186/s40645-016-0109-2, 2016.

Peng, J. F., Hu, M., Wang, Z. B., Huang, X. F., Kumar, P., Wu, Z. J., Guo, S., Yue, D. L., Shang, D. J., Zheng, Z., and He, L. Y.: Submicron aerosols at thirteen diversified sites in China: size distribution, new particle formation and corresponding contribution to cloud condensation nuclei production, Atmospheric Chemistry and Physics, 14, 10249-10265, 10.5194/acp-14-10249-2014, 2014.

Petters, M. D., and Kreidenweis, S. M.: A single parameter representation of hygroscopic growth and cloud condensation nucleus activity, Atmos. Chem. Phys., 7, 1961-1971, 10.5194/acp-7-1961-2007, 2007.

Pierce, J. R., Leaitch, W. R., Liggio, J., Westervelt, D. M., Wainwright, C. D., Abbatt, J. P. D., Ahlm, L., Al-Basheer, W., Cziczo, D. J., Hayden, K. L., Lee, A. K. Y., Li, S. M., Russell, L. M., Sjostedt, S. J., Strawbridge, K. B., Travis, M., Vlasenko, A., Wentzell, J. J. B., Wiebe, H. A., Wong, J. P. S., and Macdonald, A. M.: Nucleation and condensational growth to CCN sizes during a sustained pristine biogenic SOA event in a forested mountain valley, Atmos. Chem. Phys., 12, 3147-3163, 10.5194/acp-12-3147-2012, 2012.

Rodríguez, S., González, Y., Cuevas, E., Ramos, R., Romero, P. M., Abreu-Afonso, J., and Redondas, A.: Atmospheric nanoparticle observations in the low free troposphere during upward orographic flows at Izaña Mountain Observatory, Atmos. Chem. Phys., 9, 6319-6335, 10.5194/acp-9-6319-2009, 2009.

775 Rose, C., Sellegri, K., Freney, E., Dupuy, R., Colomb, A., Pichon, J. M., Ribeiro, M., Bourianne, T., Burnet,
776 F., and Schwarzenboeck, A.: Airborne measurements of new particle formation in the free troposphere
777 above the Mediterranean Sea during the HYMEX campaign, Atmospheric Chemistry and Physics, 15,
778 10203-10218, 10.5194/acp-15-10203-2015, 2015.

779 Shen, X., Sun, J., Zhang, X., Kivekäs, N., Zhang, Y., Wang, T., Zhang, X., Yang, Y., Wang, D., Zhao, Y., and
780 Qin, D.: Particle Climatology in Central East China Retrieved from Measurements in Planetary Boundary
781 Layer and in Free Troposphere at a 1500-m-High Mountaintop Site, Aerosol and Air Quality Research,
782 16, 659-701, 10.4209/aaqr.2015.02.0070, 2016.

783 Shen, X. J., Sun, J. Y., Zhang, Y. M., Wehner, B., Nowak, A., Tuch, T., Zhang, X. C., Wang, T. T., Zhou, H. G.,
784 Zhang, X. L., Dong, F., Birmili, W., and Wiedensohler, A.: First long-term study of particle number size
785 distributions and new particle formation events of regional aerosol in the North China Plain,
786 Atmospheric Chemistry and Physics, 11, 1565-1580, 10.5194/acp-11-1565-2011, 2011.

787 Sipilä, M., Berndt, T., Petäjä, T., Brus, D., Vanhanen, J., Stratmann, F., Patokoski, J., Mauldin, R. L.,
788 Hyvärinen, A.-P., Lihavainen, H., and Kulmala, M.: The Role of Sulfuric Acid in Atmospheric Nucleation,
789 Science, 327, 1243-1246, 10.1126/science.1180315, 2010.

790 Tan, P. Q., Li, Y., Hu, Z. Y., and Lou, D. M.: Investigation of nitrogen oxides, particle number, and size
791 distribution on a light-duty diesel car with B10 and G10 fuels, Fuel, 197, 373-387, 2017.

792 Tröstl, J., Chuang, W. K., Gordon, H., Heinritzi, M., Yan, C., Molteni, U., Ahlm, L., Frege, C., Bianchi, F.,
793 Wagner, R., Simon, M., Lehtipalo, K., Williamson, C., Craven, J. S., Duplissy, J., Adamov, A., Almeida, J.,
794 Bernhammer, A.-K., Breitenlechner, M., Brilke, S., Dias, A., Ehrhart, S., Flagan, R. C., Franchin, A., Fuchs,
795 C., Guida, R., Gysel, M., Hansel, A., Hoyle, C. R., Jokinen, T., Junninen, H., Kangasluoma, J., Keskinen, H.,
796 Kim, J., Krapf, M., Kürten, A., Laaksonen, A., Lawler, M., Leiminger, M., Mathot, S., Möhler, O., Nieminen,
797 T., Onnela, A., Petäjä, T., Piel, F. M., Miettinen, P., Rissanen, M. P., Rondo, L., Sarnela, N., Schobesberger,
798 S., Sengupta, K., Sipilä, M., Smith, J. N., Steiner, G., Tomè, A., Virtanen, A., Wagner, A. C., Weingartner,
799 E., Wimmer, D., Winkler, P. M., Ye, P., Carslaw, K. S., Curtius, J., Dommen, J., Kirkby, J., Kulmala, M.,
800 Riipinen, I., Worsnop, D. R., Donahue, N. M., and Baltensperger, U.: The role of low-volatility organic
801 compounds in initial particle growth in the atmosphere, Nature, 533, 527-531, 10.1038/nature18271,
802 2016a.

803 Tröstl, J., Herrmann, E., Frege, C., Bianchi, F., Molteni, U., Bukowiecki, N., Hoyle, C. R., Steinbacher, M.,
804 Weingartner, E., Dommen, J., Gysel, M., and Baltensperger, U.: Contribution of new particle formation
805 to the total aerosol concentration at the high-altitude site Jungfraujoch (3580 m asl, Switzerland),
806 Journal of Geophysical Research: Atmospheres, 121, 11,692-611,711, 10.1002/2015jd024637, 2016b.

807 Vu, T. V., Delgado-Saborit, J. M., and Harrison, R. M.: Review: Particle number size distributions from
808 seven major sources and implications for source apportionment studies, Atmospheric Environment, 122,
809 114-132, 2015.

810 Wang, Z., Wu, Z., Yue, D., Shang, D., Guo, S., Sun, J., Ding, A., Wang, L., Jiang, J., Guo, H., Gao, J., Cheung,
811 H. C., Morawska, L., Keywood, M., and Hu, M.: New particle formation in China: Current knowledge and
812 further directions, The Science of the total environment, 577, 258-266, 10.1016/j.scitotenv.2016.10.177,
813 2017.

814 Wang, Z. B., Hu, M., Yue, D. L., Zheng, J., Zhang, R. Y., Wiedensohler, A., Wu, Z. J., Nieminen, T., and Boy,
815 M.: Evaluation on the role of sulfuric acid in the mechanisms of new particle formation for Beijing case,
816 Atmospheric Chemistry and Physics, 11, 12663-12671, 10.5194/acp-11-12663-2011, 2011.

817 Wang, Z. B., Hu, M., Sun, J. Y., Wu, Z. J., Yue, D. L., Shen, X. J., Zhang, Y. M., Pei, X. Y., Cheng, Y. F., and
818 Wiedensohler, A.: Characteristics of regional new particle formation in urban and regional background

819 environments in the North China Plain, Atmospheric Chemistry and Physics, 13, 12495-12506,
820 10.5194/acp-13-12495-2013, 2013a.

821 Wang, Z. B., Hu, M., Wu, Z. J., Yue, D. L., He, L. Y., Huang, X. F., Liu, X. G., and Wiedensohler, A.: Long-
822 term measurements of particle number size distributions and the relationships with air mass history
823 and source apportionment in the summer of Beijing, Atmospheric Chemistry and Physics, 13, 10159-
824 10170, 10.5194/acp-13-10159-2013, 2013b.

825 Weller, R., Schmidt, K., Teinilä, K., and Hillamo, R.: Natural new particle formation at the coastal Antarctic
826 site Neumayer, Atmospheric Chemistry and Physics, 15, 11399-11410, 10.5194/acp-15-11399-2015,
827 2015.

828 Wu, Z., Hu, M., Liu, S., Wehner, B., Bauer, S., Ma ßling, A., Wiedensohler, A., Petäjä, T., Dal Maso, M.,
829 and Kulmala, M.: New particle formation in Beijing, China: Statistical analysis of a 1-year data set,
830 Journal of Geophysical Research, 112, 10.1029/2006jd007406, 2007.

831 Wu, Z., Hu, M., Lin, P., Liu, S., Wehner, B., and Wiedensohler, A.: Particle number size distribution in the
832 urban   atmosphere   of   Beijing,   China,   Atmospheric   Environment,   42,   7967-7980,
833 10.1016/j.atmosenv.2008.06.022, 2008.

834 Wu, Z. J., Poulain, L., Henning, S., Dieckmann, K., Birmili, W., Merkel, M., van Pinxteren, D., Spindler, G.,
835 Müller, K., Stratmann, F., Herrmann, H., and Wiedensohler, A.: Relating particle hygroscopicity and CCN
836 activity to chemical composition during the HCCT-2010 field campaign, Atmos. Chem. Phys., 13, 7983-
837 7996, 10.5194/acp-13-7983-2013, 2013.

838 Wu, Z. J., Zheng, J., Shang, D. J., Du, Z. F., Wu, Y. S., Zeng, L. M., Wiedensohler, A., and Hu, M.: Particle
839 hygroscopicity and its link to chemical composition in the urban atmosphere of Beijing, China, during
840 summertime, Atmos. Chem. Phys., 16, 1123-1138, 10.5194/acp-16-1123-2016, 2016.

841 Xu, J., Wang, Z., Yu, G., Qin, X., Ren, J., and Qin, D.: Characteristics of water soluble ionic species in fine
842 particles from a high altitude site on the northern boundary of Tibetan Plateau: Mixture of mineral dust
843 and anthropogenic aerosol, Atmospheric Research, 143, 43-56, 10.1016/j.atmosres.2014.01.018, 2014.

844 Xu, J. Z., Zhang, Q., Wang, Z. B., Yu, G. M., Ge, X. L., and Qin, X.: Chemical composition and size
845 distribution of summertime PM2.5 at a high altitude remote location in the northeast of the Qinghai–
846 Xizang (Tibet) Plateau: insights into aerosol sources and processing in free troposphere, Atmospheric
847 Chemistry and Physics, 15, 5069-5081, 10.5194/acp-15-5069-2015, 2015.

848 Yli-Juuti, T., Riipinen, I., Aalto, P. P., Nieminen, T., Maenhaut, W., Janssens, I. A., Claeys, M., Salma, I.,
849 Ocskay, R., Hoffer, A., Imre, K., and Kulmala, M.: Characteristics of new particle formation events and
850 cluster ions at K-puszta, Hungary, Boreal Environ. Res., 14, 683-698, 2009.

851 Yu, F., and Hallar, A. G.: Difference in particle formation at a mountaintop location during spring and
852 summer: Implications for the role of sulfuric acid and organics in nucleation, Journal of Geophysical
853 Research: Atmospheres, 119, 12,246-212,255, 10.1002/2014jd022136, 2014.

854 Yue, D. L., Hu, M., Zhang, R. Y., Wang, Z. B., Zheng, J., Wu, Z. J., Wiedensohler, A., He, L. Y., Huang, X. F.,
855 and Zhu, T.: The roles of sulfuric acid in new particle formation and growth in the mega-city of Beijing,
856 Atmospheric Chemistry And Physics, 10, 4953-4960, 10.5194/acp-10-4953-2010, 2010.

857 Zellweger, C., Forrer, J., Hofer, P., Nyeki, S., Schwarzenbach, B., Weingartner, E., Ammann, M., and
858 Baltensperger, U.: Partitioning of reactive nitrogen (NOy) and dependence on meteorological conditions
859 in the lower free troposphere, Atmos. Chem. Phys., 3, 779-796, 10.5194/acp-3-779-2003, 2003.

860 Zhang, R., Khalizov, A., Wang, L., Hu, M., and Xu, W.: Nucleation and growth of nanoparticles in the
861 atmosphere, Chemical reviews, 112, 1957-2011, 10.1021/cr2001756, 2012.

862 Zhang, X., Yin, Y., Lin, Z., Han, Y., Hao, J., Yuan, L., Chen, K., Chen, J., Kong, S., Shan, Y., Xiao, H., and Tan,

863   W.: Observation of aerosol number size distribution and new particle formation at a mountainous site
864   in Southeast China, The Science of the total environment, 575, 309-320,
865   10.1016/j.scitotenv.2016.09.212, 2016.
866   Zheng, J., Hu, M., Peng, J., Wu, Z., Kumar, P., Li, M., Wang, Y., and Guo, S.: Spatial distributions and
867   chemical properties of PM2.5 based on 21 field campaigns at 17 sites in China, Chemosphere, 159, 480-
868   487, 10.1016/j.chemosphere.2016.06.032, 2016.
869   Zheng, J., Hu, M., Du, Z., Shang, D., Gong, Z., Qin, Y., Fang, J., Gu, F., Li, M., Peng, J., Li, J., Zhang, Y., Huang,
870   X., He, L., Wu, Y., and Guo, S.: Influence of biomass burning from South Asia at a high-altitude mountain
871   receptor site in China, Atmos. Chem. Phys., 17, 6853-6864, 10.5194/acp-17-6853-2017, 2017.

872

873

Table 1. Densities and hygroscopic parameters of the compounds used in CCN

calculation

Species	NH_4NO_3	NH_4HSO_4	$(NH_4)_2SO_4$	H_2SO_4	Organics	BC
ρ (kg m^{-3})	1720	1780	1769	1830	1400	1700
κ	0.67	0.61	0.61	0.91	0.1	0

Table 2. Particle number concentration of high altitude sites around the world, in

comparison with this study

Location	Altitude [m]	Date	Size range [nm]	PN [cm^{-3}]	Reference
Sierra Nevada Mountains, US	1315	May-Nov 2002	10-400	4300	(Lunden et al., 2006)
Mt. Tai, China	1534	July 2010-Feb 2012	3-2500	11800±6200	(Shen et al., 2016)
Mt. Huang, China	1840	April-Aug 2008	10-10000	2350	(Zhang et al., 2016)
Mukteshwar, India	2180	Nov 2005-Nov 2008	10-800	2730	(Komppula et al., 2009)
Izana Observatory, Spain	2367	Nov 2006-Dec 2007	3-660	480-4600	(Rodríguez et al., 2009)
Mt. Norikura, Japan	2770	Sep 2001, July-Sep 2002	9-300	260-1600	(Nishita et al., 2008)
University of Colorado Mountain Research Station, US	2900	July 2006	3-800	2881-19947	(Boy et al., 2008)
Dome C, Antarctica	3200	Spring, 2008-2009	10-600	17.9-457	(Järvinen et al., 2013)
Storm Peak Laboratory, US	3210	Mar 2012	10-10000	3100	(Yu and Hallar, 2014)
Jungfraujoch, Switzerland	3580	1995-2015	10-10000	757	(Bukowiecki et al., 2016)
Wangliguan, China	3816	Sep 2005-May 2007	12-570	2030	(Kivekäs et al., 2009)
Mt. Daban, China	3295	Sep-October 2013	12-478	2300	(Du et al., 2015)
Mt. Yulong, China	3410	May-April 2015	3-10000	1600±1290	This Study

884 **Table 3. Fitted parameters of lognormal modes for different period. μ, σ and N**

885 **represent the mean diameter, standard deviation, and total number concentration**

886 **of each mode, respectively. "Total" represents the mean result of all data achieved**

887 **from the campaign.**

Period	μ [nm]			σ [nm]			N [cm^{-3}]		
	mode_1	mode_2	mode_3	mode_1	mode_2	mode_3	mode_1	mode_2	mode_3
Total	16	52	130	1.75	1.75	1.77	221	488	861
BB1	23	92	169	1.94	1.91	1.63	428	1014	744
BB2	16	47	106	1.75	1.75	1.75	117	302	775
BB3	15	70	130	1.75	1.75	1.72	106	1309	628
BG	15	79	-	2.03	1.73	-	301	368	-

888

889 **Table 4. Comparisons of NPF parameters (FR, GR, CS) with the other studies.**

Site	Region	Altitude [m]	Size [nm]	FR [cm^{-3}s^{-1}]	GR [nm h^{-1}]	CS [s^{-1}]	Reference
Mt. Yulong	Asia	3410	3-25	1.18	3.22	0.002	This research
Mukteshwar	Asia	2180	15-20	0.44	2.47	0.015	(Neitola et al., 2011)
Storm peak laboratory	North America	3210	9-334	0.39	7.5	0.001	(Hallar et al., 2011)
Mt. Tai	Asia	1500	3-25	4	6.1	0.02	(Shen et al., 2016)
Izaña	Atlantic Ocean	2400	10-25	0.46	0.43	0.002	(García et al., 2014)
Jungfraujoch	Europe	3580	3.2-15	1.8	4.0	-	(Tröstl et al., 2016b)
Dome C	Antarctica	3200	10-25	0.023	2.5	0.0002	(Järvinen et al., 2013)

890

891
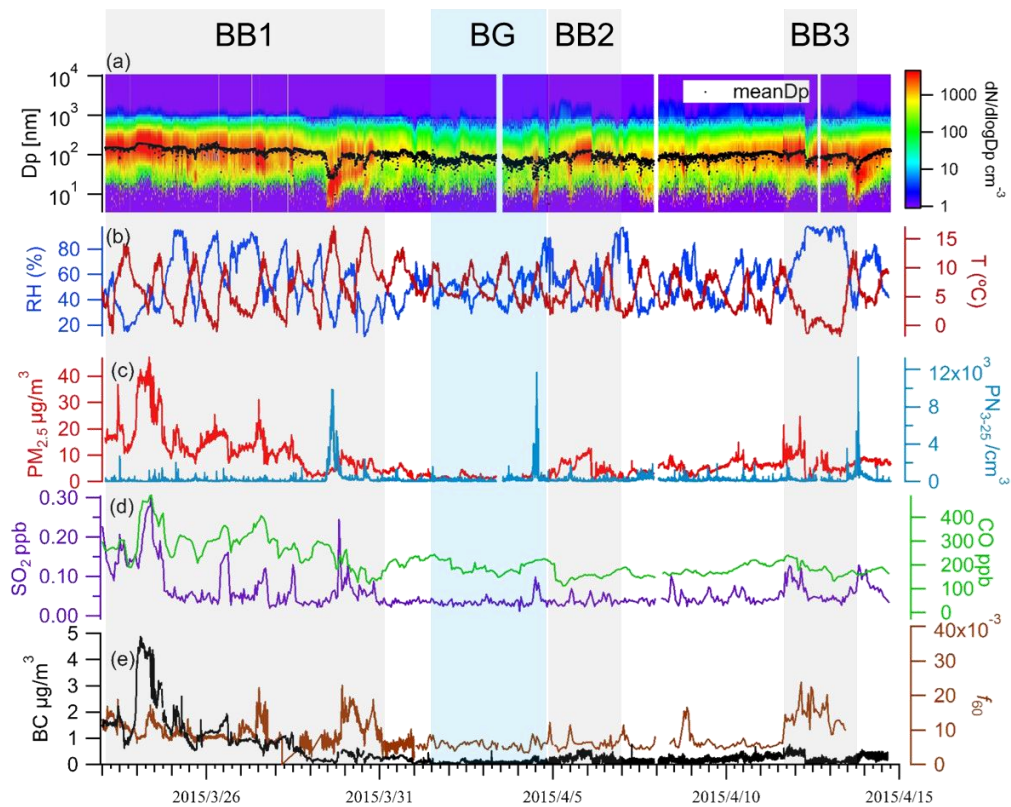
Figure 1. Time series of (a) particle number size distribution and geometric mean diameter, (b) ambient temperature, relative humidity, (c) PM$_{2.5}$ mass concentration, number concentration of nucleation mode (3-25 nm) particles (PN$_{3-25}$), (d) SO$_2$ and CO concentration, (e) black carbon concentration, fraction of f60 (organic fragment ions with m/z=60) during the monitoring campaign. Periods influenced by biomass burning (BB1, BB2, BB3) were marked by grey shades, period representing background condition (BG) was marked by blue shade.

899
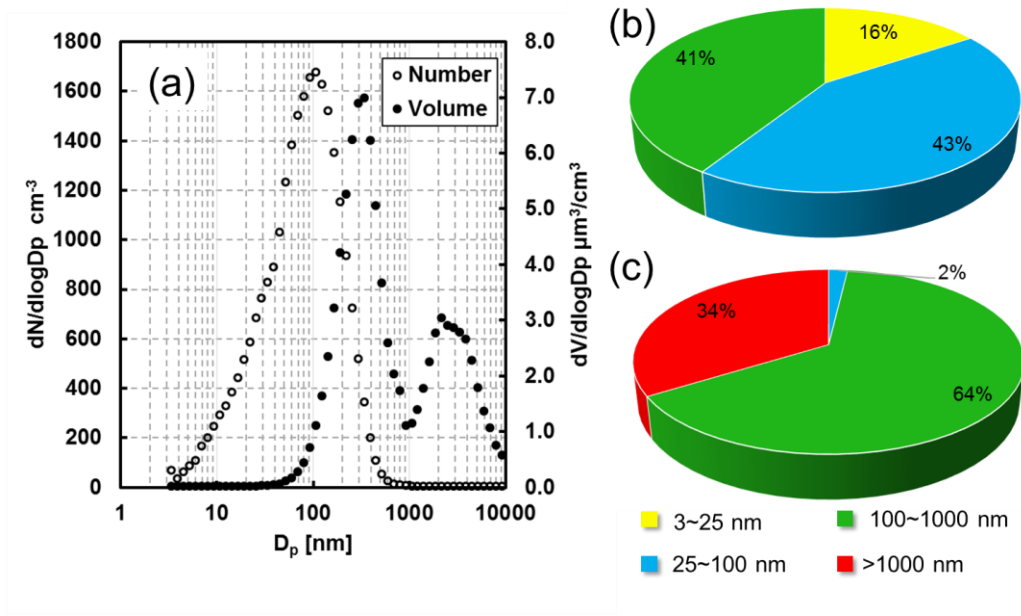
Figure 2. Particle size distribution in atmosphere at Mt. Yulong. (a) Mean size distribution of particle number (hollow circle) and volume (filled circle) concentration; Contribution of different fractions to total particle (b) number concentration and (c) volume concentration. Different colors represent different size ranges: yellow (3-25 nm), blue (25-100 nm), green (100-1000 nm), red (1-10 μm).
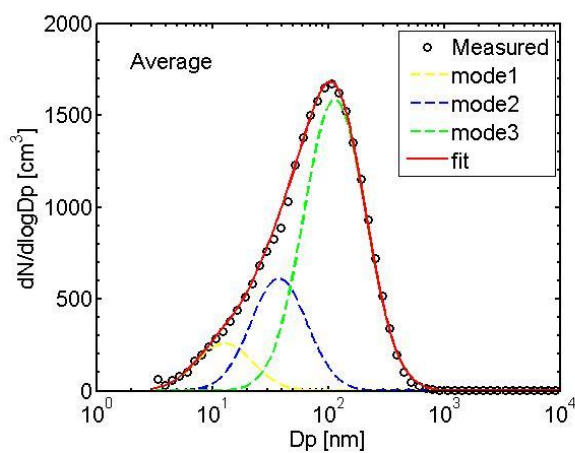
Figure 3. Lognormal fit (3 modes) of average particle number size distribution during the campaign at Mt. Yulong. Black circles mark the measured PNSD, colored dash lines represent the PNSD of fitting modes, and red full line marks the sum of PNSD of all fitting modes. Mode 1, 2 and 3 were nucleation mode, Aitken mode and accumulation mode, respectively.

913

914
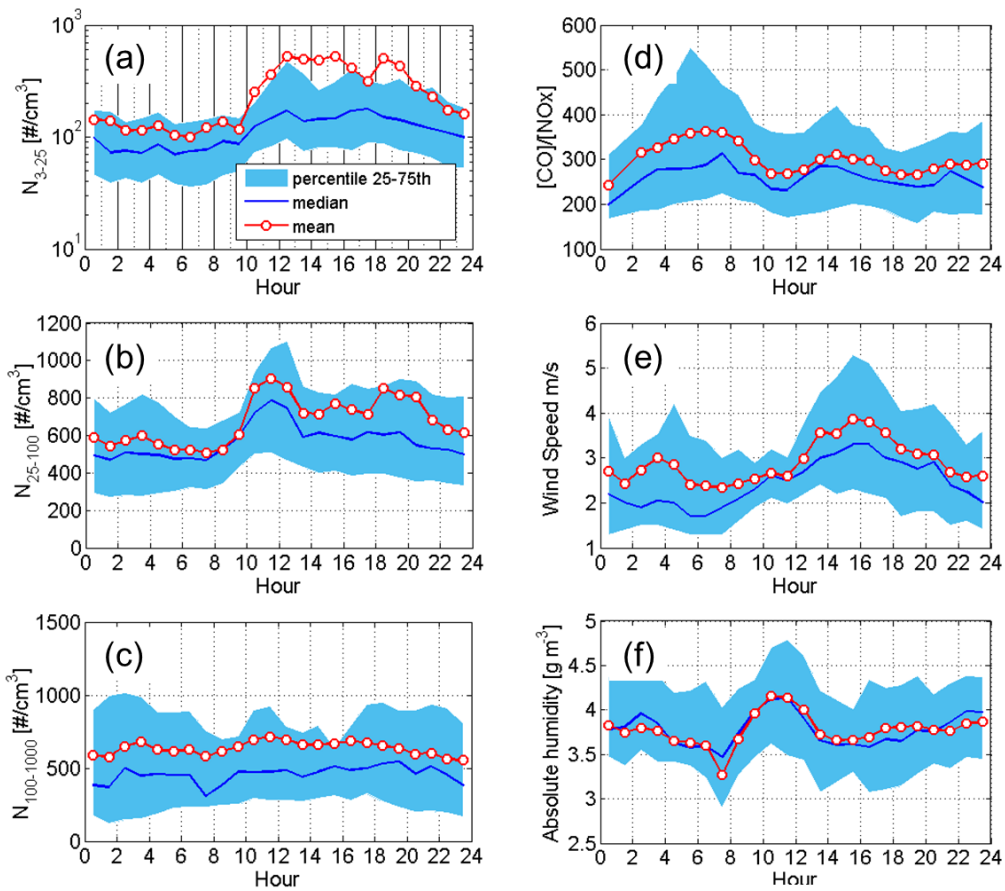
Figure 4. Diurnal variations of N_{3-25}, N_{25-100}, $N_{100-1000}$, CO/NO$_x$, wind speed, and absolute humidity at Mt. Yulong during monitoring campaign. Red lines with circles, blue lines mark the mean and median results, respectively. Light blue area marks the range between 25th, and 75th percentiles of the data.

919
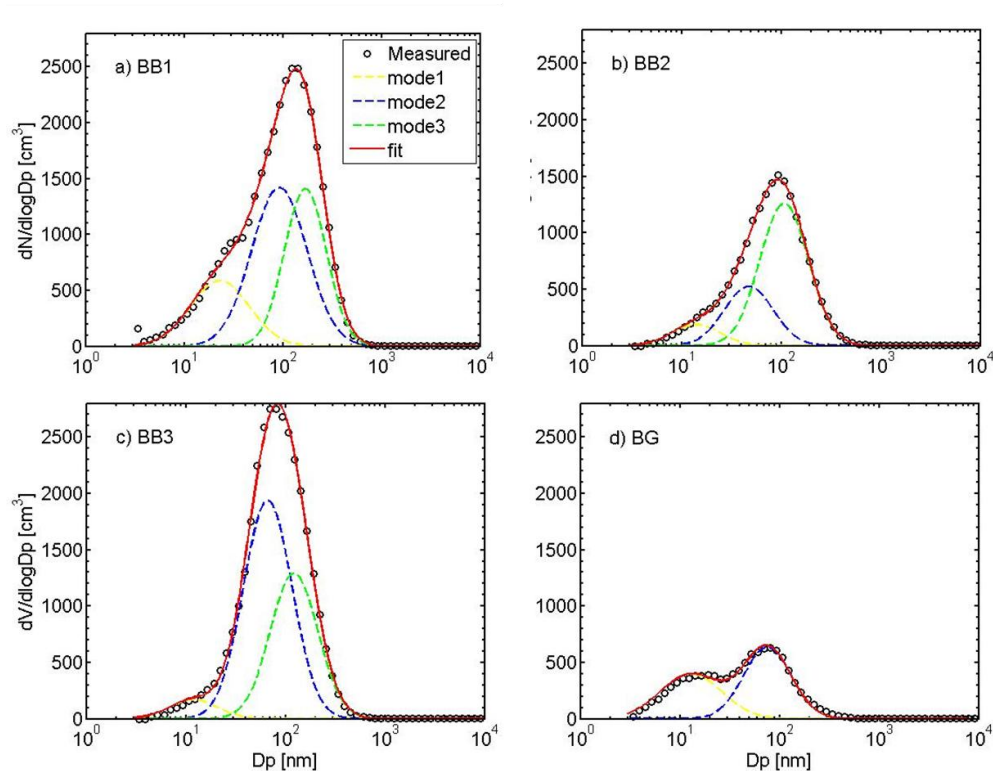
Figure 5. Lognormal fit (3 modes) of average PNSD during (a) BB1, (b) BB2, (c) BB3, (d) BG at Mt. Yulong site. Black circles mark the measured PNSD, colored dash lines represent the PNSD of fitting modes, and red full line marks the sum of PNSD of all fitting modes. Mode 1, 2, 3 were nucleation mode, Aitken mode and accumulation mode, respectively.
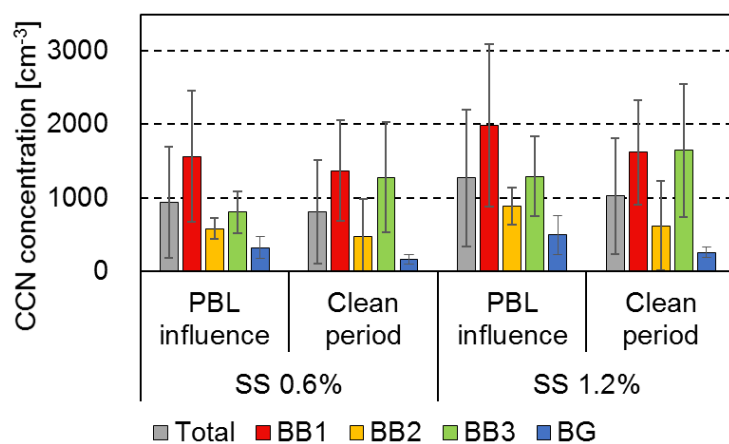
Figure 6. Mean number concentration of CCN under supersaturation of 0.6 % and 1.2 % during whole monitoring period (labelled as "total"), BB1, BB2, BB3 events (marked by shadow in Fig. 1). PBL (10:00-14:00) and FT (1:00-6:00) conditions were separated.

931

932
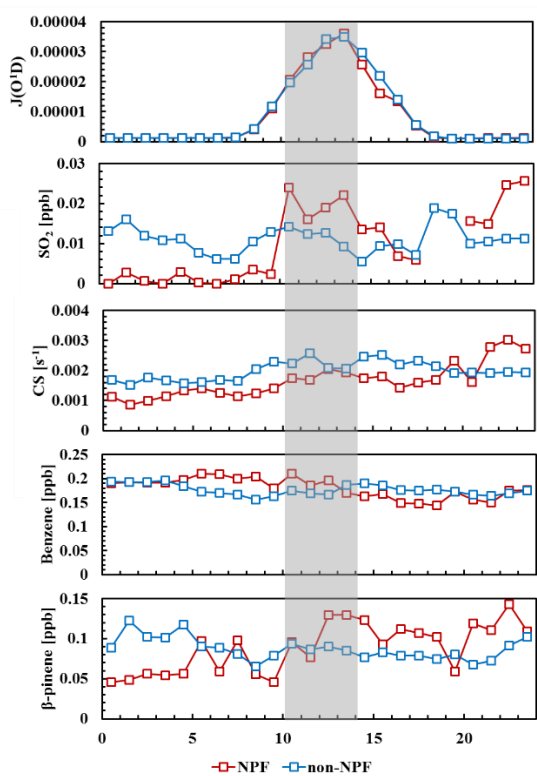
Figure 7. Diurnal variation of J(O¹D), SO₂, CS, Benzene, β-pinene during days with NPF events (labelled as "NPF", red lines with marks), and without NPF events (labelled as "non-NPF", blue lines with marks). Shadow marks the time period during which nucleation occurred.

937